AGU PUBLICATIONS

Geophysical Research Letters

RESEARCH LETTER
10.1002/2014GL061524

Key Points:
- Extratropical wind fields were derived from GPS radio occultation (RO) data
- RO geostrophic and gradient winds well represent actual 3-D wind fields
- The monthly mean RO wind fields are, in general, accurate to within 2 m/s

Correspondence to:
B. Scherllin-Pirscher,
barbara.pirscher@uni-graz.at

Citation:
Scherllin-Pirscher, B., A. K. Steiner, and G. Kirchengast (2014), Deriving dynamics from GPS radio occultation: Three-dimensional wind fields for monitoring the climate, *Geophys. Res. Lett.*, *41*, 7367–7374, doi:10.1002/2014GL061524.

Received 14 AUG 2014
Accepted 16 SEP 2014
Accepted article online 18 SEP 2014
Published online 16 OCT 2014

Deriving dynamics from GPS radio occultation: Three-dimensional wind fields for monitoring the climate

Barbara Scherllin-Pirscher[1], Andrea Karin Steiner[1], and Gottfried Kirchengast[1]

[1]Wegener Center for Climate and Global Change (WEGC) and Institute for Geophysics, Astrophysics, and Meteorology/Institute of Physics (IGAM/IP), University of Graz, Graz, Austria

Abstract Global Positioning System (GPS) radio occultation (RO) measurements are proven highly useful for observing the thermal structure of the troposphere and stratosphere. Here we use RO data for the first time to derive climatological wind fields from sampling error-corrected geopotential height fields on isobaric surfaces from about 800 hPa to 3 hPa. We find monthly mean RO geostrophic wind and gradient wind fields (2007 to 2012, about 500 km horizontal resolution, outside tropics) to clearly capture all main wind features, with differences to atmospheric analysis winds being, in general, smaller than 2 m/s. Larger differences (up to 10 m/s) occur close to the subtropical jet where RO winds underestimate actual winds. Such biases are caused by the geostrophic and gradient wind approximations, while RO retrieval errors introduce negligible effect. These results demonstrate that RO wind fields are of high quality and can provide new information on troposphere-stratosphere dynamics, for the benefit of monitoring the climate from weekly to decadal scales.

1. Introduction

Accurate knowledge of the spatial and temporal distribution of winds is required for a deeper understanding of atmospheric dynamics and chemistry and their climatic variability and change. Traditional measurements such as from radiosondes, dropsondes, or LIDAR (Light Detection and Ranging) mainly provide data over the continents in the Northern Hemisphere (NH) while coverage in the Southern Hemisphere (SH) and over oceans is poor. More homogeneous sampling is obtained from satellite measurements, but most of these data suffer from low vertical resolution [e.g., *Schmetz et al.*, 1993; *Anthes*, 2011].

Global Positioning System (GPS) radio occultation (RO) observations have the potential to overcome these problems as they globally provide soundings with high vertical resolution (from near 100 m in the lower troposphere to about 1.5 km in the stratosphere) [*Kursinski et al.*, 1997; *Anthes*, 2011]. The GPS RO technique exploits radio signals transmitted by GPS satellites, refracted by the Earth's atmosphere, and received by a low Earth orbit satellite. These measurements provide accurate and precise information on the thermodynamic state of the atmosphere, including temperature and pressure profiles, but they do not provide direct wind information. However, geopotential height of pressure levels can be derived from RO, from accurate knowledge of the refractivity probed by the GPS signals and of the satellite positions and velocities involved [*Leroy*, 1997]. Since validation of RO geopotential height fields provided proof of their high quality [*Leroy*, 1997; *Scherllin-Pirscher et al.*, 2011; *Steiner et al.*, 2013], these fields can consequently be used to infer wind fields.

In the recent decades many studies were performed to investigate the validity of geostrophic and gradient wind approximations in the troposphere and stratosphere [e.g., *Boville*, 1987; *Randel*, 1987]. The geostrophic approximation is the simplest method for estimating winds from geopotential height fields as it balances the pressure gradient force and Coriolis force [*Holton and Hakim*, 2012]. This approximation is reasonable in the middle and upper troposphere at subtropical and mid-latitudes. Gradient winds in addition include the centrifugal force and are a good approximation also in the polar stratosphere [*Randel*, 1987]. These results were confirmed by analyses of geostrophic and gradient winds from satellites in the stratosphere, mesosphere, and lower thermosphere [*Lieberman*, 1999; *Oberheide et al.*, 2002; *Smith and Gille*, 2014].

Verkhoglyadova et al. [2014] simulated GPS RO measurements and showed that monthly mean geostrophic winds near the tropopause can be obtained with an accuracy of within about 4 m/s. They attributed the

dominant errors to ageostrophy, such as from vertical momentum fluxes and convergence/divergence of wave momentum fluxes, and to undersampling of the "true" atmospheric state by the RO profiles (sampling error).

In this study, we present for the first time RO-derived climatological winds in the troposphere to lower stratosphere based on real RO measurements over 2007 to 2012. We compute these RO winds from sampling error-corrected monthly mean geopotential height fields (section 2), validate them with atmospheric analyses (section 3), and finally summarize and conclude (section 4).

2. Derivation of Wind Fields From GPS RO

GPS RO measurements provide near-vertical profiles of atmospheric refractivity. In dry atmosphere regions (above the lower to middle troposphere), refractivity is directly proportional to density and RO (dry) pressure is derived by downward integration of density assuming hydrostatic equilibrium [e.g., *Kursinski et al.*, 1997]. In moist tropospheric regions, refractivity also depends on water vapor and the retrieval of RO (physical) pressure also needs an a priori knowledge of temperature and/or humidity. The differences between RO-derived dry and physical (actual) pressure profiles in the troposphere are explained in detail by *Scherllin-Pirscher et al.* [2011].

Geopotential height from RO data is obtained based on the accurate knowledge of refractivity and of the positions and velocities of the satellites involved [*Leroy*, 1997]. Thus, as a unique feature of the RO method, geopotential height profiles $Z(z_i)$ are explicitly available together with pressure profiles $p(z_i)$, on a joint altitude grid z_i and essentially only depending on GPS signal refraction and orbit data so that very accurate profiles of geopotential height as function of pressure $Z(p)$ can be exploited.

For this study we used $Z(p)$ profiles from four RO satellite missions: Challenging Minisatellite Payload (CHAMP) [*Wickert et al.*, 2001], Satélite de Aplicaciones Científicas (SAC-C) [*Hajj et al.*, 2004], Gravity Recovery And Climate Experiment (GRACE-A) [*Wickert et al.*, 2005], and Formosa Satellite Mission 3/Constellation Observing System for Meteorology, Ionosphere, and Climate (Formosat-3/COSMIC) [*Anthes et al.*, 2008] for the period January 2007 to December 2012, providing on average more than 55,000 RO profiles per month. All these $Z(p)$ profiles (with p the actual physical pressure) were retrieved with the Wegener Center Occultation Processing System version 5.6 (WEGC OPSv5.6) [*Schwärz et al.*, 2013], which is an enhanced version of the WEGC OPSv5.4, described in detail by *Ho et al.* [2012] and *Steiner et al.* [2013]. In the WEGC OPSv5.6 background information is included at high altitudes (down to 30 km) at bending angle level. The investigated RO satellite climatologies are dominated by the observations up to about 10 hPa. The OPSv5.6 processing includes a quality control with plausibility checks of bending angle, refractivity, and temperature profiles [*Schwärz et al.*, 2013]. For this study we only used profiles which passed the quality control.

Individual profiles were interpolated linearly in the logarithm of pressure to a common vertical pressure grid p_i, which was defined as a regular 200 m "log-pressure" altitude grid $z_{p,i}$ from 1.6 km to 40.0 km. It was obtained from $p_i = p_{\mathrm{surf}}\exp(-z_{p,i}/H)$, where $p_{\mathrm{surf}} = 1013.25$ hPa is standard surface pressure and $H = 7$ km a standard scale height. Thus, p_i ranges in 193 levels from 806.2 hPa to 3.34 hPa (corresponding to about 2 km to 40 km in altitude).

Averaging over all individual geopotential height profiles available within any given month, monthly means were calculated for 5° × 5° equal-area bins, with the area defined by the near-equator bins in 0° to 5°N/S. Thus, keeping the latitudinal width of bins fixed at 5°, their longitudinal width increases with latitude, leading to considerably bin overlapping at polar latitudes and a horizontal resolution of about 500 km everywhere.

RO measurements are of very high quality in the upper troposphere and lower stratosphere (UTLS), but RO climatological fields are affected by errors including statistical (random) error, systematic error, or sampling error [*Scherllin-Pirscher et al.*, 2011]. The statistical error effectively diminishes due to averaging over a large number of profiles. In the UTLS region and outside the tropics (smallest number of RO measurements per surface area), the geopotential height statistical error is generally smaller than 2 m for 5° × 5° equal-area bins. The geopotential height systematic error, which results from the measurements and from assumptions made in the RO data processing, was estimated to no more than 7 m in the UTLS [*Scherllin-Pirscher et al.*, 2011].

RO climatologies are also affected by a sampling error, which results from undersampling the true horizontal variability by the discrete times and locations of individual RO measurements [*Pirscher et al.*, 2007]. Several studies showed that the sampling error can be robustly estimated and subtracted when using RO climatological fields [see, e.g., *Foelsche et al.*, 2011; *Steiner et al.*, 2011, 2013]. Following these studies, we used operational European Centre for Medium-Range Weather Forecasts (ECMWF) analysis fields, estimated the sampling error, and subtracted it from the RO geopotential height climatologies on a monthly basis. The remaining residual sampling error is small (less than 30% of the original sampling error) [*Scherllin-Pirscher et al.*, 2011] and lies generally within 10 m in the UTLS.

Geostrophic wind was obtained from monthly mean sampling error-corrected 5° × 5° geopotential height climatologies using [e.g., *Holton and Hakim*, 2012]

$$u_{geo} = -\frac{1}{f(\varphi)}\frac{1}{R_E}\frac{\partial \Phi}{\partial \varphi} \tag{1}$$

and

$$v_{geo} = \frac{1}{f(\varphi)}\frac{1}{R_E \cos\varphi}\frac{\partial \Phi}{\partial \lambda}, \tag{2}$$

where u_{geo} and v_{geo} are zonal and meridional components of geostrophic wind, respectively, $f(\varphi) = 2\Omega \sin\varphi$ is the local Coriolis parameter, Ω the Earth's rotation rate (7.2921×10^{-5} rad/s), R_E the mean radius of the Earth (6371.0 km), φ latitude, λ longitude, and $\Phi = Zg_0$ the geopotential, with g_0 being the global standard gravity at mean sea level (9.80665 m/s^2).

Subsequently, we estimated the gradient wind from the same geopotential height climatologies. While the geostrophic wind approximation assumes a balance of the pressure gradient force and the Coriolis force, gradient winds also include the centrifugal force. The zonal gradient wind component u_{grad} was derived based on *Randel* [1987],

$$u_{grad} = \frac{-f(\varphi) \pm \sqrt{f^2(\varphi) + 4f(\varphi)u_{geo}\tan\varphi/R_E}}{2\tan\varphi/R_E}, \tag{3}$$

where the ± sign in the numerator applies to the Northern/Southern Hemisphere. The meridional gradient wind component v_{grad} was obtained according to *Oberheide et al.* [2002],

$$v_{grad} = \frac{v_{geo} f(\varphi)}{f(\varphi) + u_{grad}\tan\varphi/R_E}. \tag{4}$$

Since the Coriolis parameter $f(\varphi)$ vanishes at the equator, geostrophic and gradient winds were investigated only outside the tropics (poleward of 15°S/N; first center latitudes of bins at 17.5°S/N).

In order to obtain error estimates for our monthly mean geostrophic and gradient winds, we compared them to winds from monthly mean ECMWF analysis fields used at ~300 km horizontal resolution (comparable to horizontal resolution of RO). Furthermore, we computed ECMWF geostrophic and gradient winds and differences between these wind approximations and the ECMWF true wind. These differences give a measure for the errors induced by the geostrophic and gradient wind approximations. Differences between RO geostrophic/gradient winds relative to ECMWF geostrophic/gradient winds were used to estimate RO retrieval errors.

3. Validation of GPS RO Wind Fields

RO-derived geopotential height of isobaric surfaces and geostrophic winds are very reasonable as illustrated in Figure 1 for January 2009. At the 200 hPa pressure level geopotential height at NH (winter) polar latitudes is smaller than 11 km increasing to about 12 km at mid-latitudes. Stationary waves yield a wave-like pattern, and geostrophic wind smoothly follows geopotential height isolines in an eastward direction. In the SH summer, geopotential height is higher than in the NH winter, and due to smaller orographic effects, geopotential height and geostrophic winds are more symmetric.

Geostrophic wind speeds $V_{geo} = \sqrt{u_{geo}^2 + v_{geo}^2}$ at 200 hPa (Figure 2, top row) are largest in the winter hemisphere at mid-latitudes, representing the subtropical jet. In NH winter (January 2009) maximum

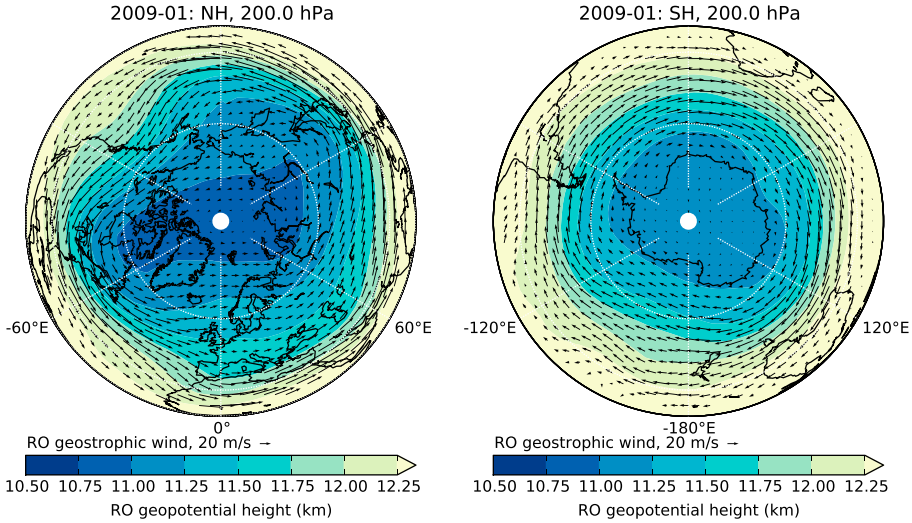

Figure 1. (left) Northern Hemisphere and (right) Southern Hemisphere RO geopotential height (colored contours) and geostrophic wind (vector symbols) at 200 hPa in January 2009 from the pole to the tropics.

monthly mean wind speed (>60 m/s) is found at 30°N above East Asia and the western Pacific. In SH winter (July 2009), maximum wind speed is slightly smaller (<60 m/s) but more symmetric than in the NH.

Differences between RO geostrophic/gradient wind and actual wind from ECMWF analyses (Figure 2, middle and bottom rows) are, in general, within ±2 m/s. Larger differences (mainly between 4 m/s and 8 m/s) are found at mid-latitudes close to the subtropical jet, where RO-derived winds

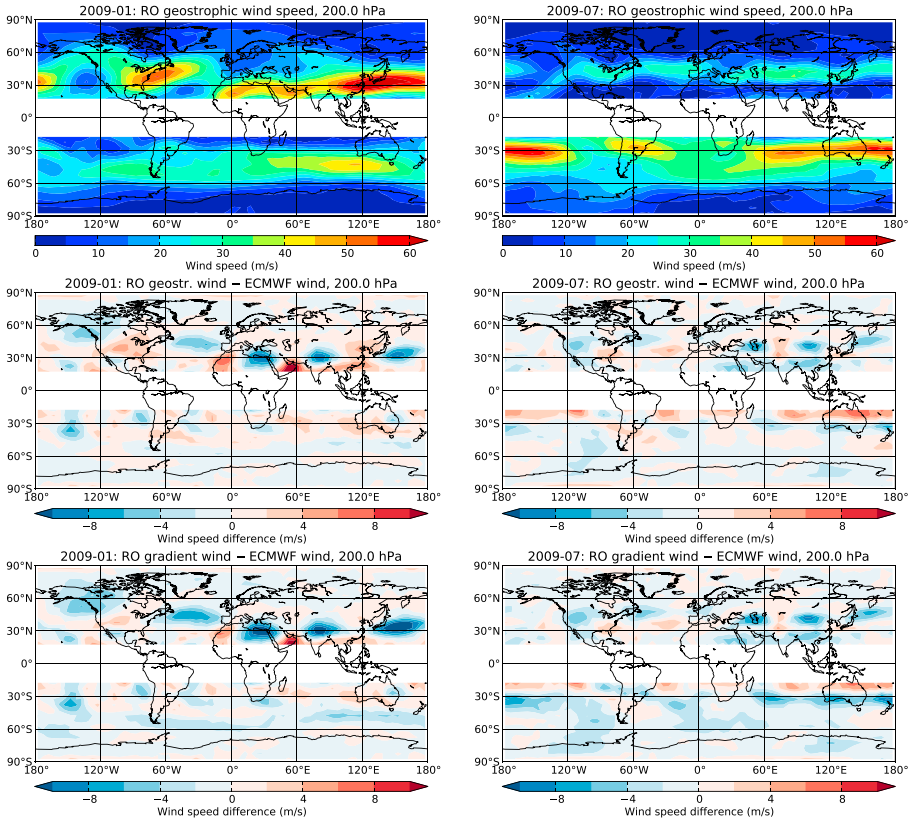

Figure 2. Geographic maps (outside the tropics) of (top row) RO geostrophic wind speed, (middle row) its difference to ECMWF wind speed, and (bottom row) difference between RO gradient wind speed and ECMWF wind speed, at 200 hPa in January 2009 (left column) and July 2009 (right column).

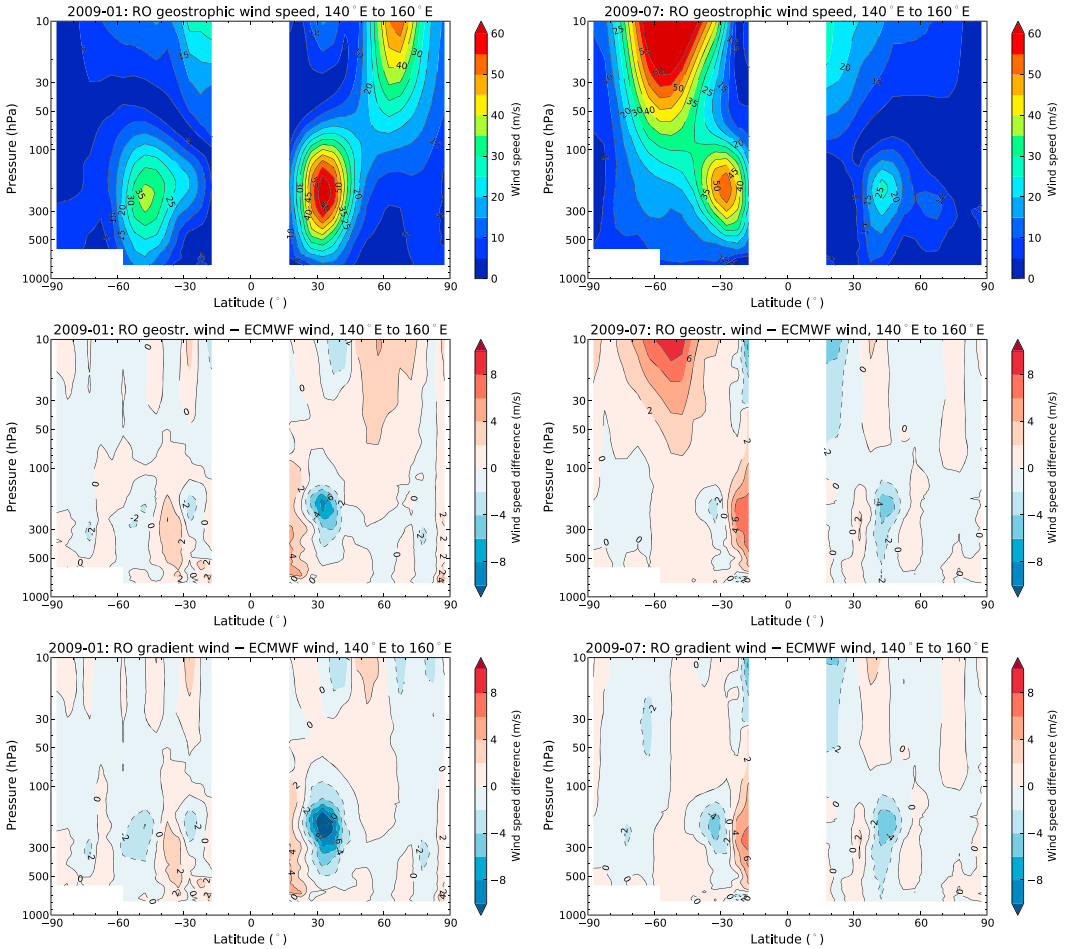

Figure 3. Latitude-altitude cross sections (outside the tropics) of (top row) RO geostrophic wind speed, (middle row) its difference to ECMWF wind speed, and (bottom row) difference between RO gradient wind speed and ECMWF wind speed, averaged over 140°E to 160°E in January 2009 (left column) and July 2009 (right column).

underestimate actual winds. These biases tend to be slightly larger for gradient winds than for geostrophic winds. Our error analysis revealed that the differences are caused by the geostrophic and gradient wind approximations while the effect of RO retrieval errors is small (<2 m/s).

A meridional cross section (over the western Pacific) of geostrophic wind and differences between RO geostrophic wind/gradient wind and ECMWF is shown in Figure 3. Due to the decreasing number of RO profiles covering the lower troposphere, we did not analyze results below 800 hPa (and below 600 hPa above Antarctica; 60°S to 90°S). Largest wind speeds (>60 m/s) are again evident at winter mid-latitudes close to the tropopause but also in the winter hemisphere above approximately 50 hPa (polar night jet).

Notable biases are found (i) in the tropical winter troposphere up to 100 hPa (RO winds overestimate actual winds), (ii) at subtropical latitudes from approximately 150 hPa to 300 hPa (RO winds underestimate the strength of the subtropical jet), and (iii) in the lower winter stratosphere above 50 hPa, where RO geostrophic wind overestimates the strength of the polar night jet. This latter bias is substantially reduced for the RO gradient wind. Even the large stratospheric warming event end of January 2009 [*Harada et al.*, 2010] (which was accompanied by intense wave activity) did not notably affect the gradient wind approximation, and differences to ECMWF remain smaller than 2 m/s.

Biases of RO geostrophic/gradient wind would increase in the moist troposphere when using the RO dry pressure instead of the physical pressure as used here (cf. section 2 introduction). However, *Scherllin-Pirscher et al.* [2011] showed that outside the tropics and above an altitude of 8.5 km (approximately 300 hPa), the differences in terms of geopotential height are smaller than 10 m. We checked the subsequent differences

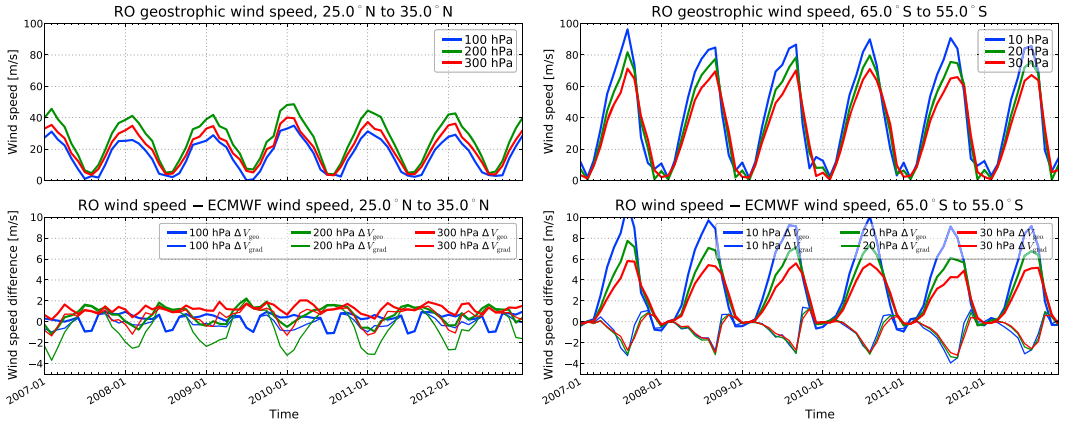

Figure 4. Time series of monthly mean zonal mean (top row) RO geostrophic wind speed and (bottom row) differences of RO geostrophic wind and RO gradient wind speed relative to ECMWF wind speed (ΔV_{geo} and ΔV_{grad}, respectively) between 25°N and 35°N (left column) for 100 hPa (blue), 200 hPa (green), and 300 hPa (red) as well as between 65°S and 55°S (right column) for 10 hPa (blue), 20 hPa (green), and 30 hPa (blue), respectively.

in RO-derived winds and found these negligible (mostly <1 m/s) above 300 hPa, a result also found by *Verkhoglyadova et al.* [2014]. Still, for optimized reach into the middle and lower troposphere, it is advisable to use the RO physical pressure.

The temporal evolution (over 2007 to 2012) of zonal mean RO geostrophic wind speed and differences between RO-derived and ECMWF wind speeds are shown in Figure 4 for the NH subtropics in the upper troposphere and SH high latitudes in the lower stratosphere. Note that the subtropical jet meanders in narrow bands in the upper troposphere (cf. Figure 2, top row) and that zonal means do not fully represent wind speeds and biases at the jet core position.

Wind speeds show a pronounced annual cycle with largest values in hemispheric winter when they exceed 40 m/s at 200 hPa in the NH subtropics and 80 m/s at 10 hPa at SH high latitudes. In the subtropical troposphere, biases are within 2 m/s except for RO gradient wind, which occasionally exhibits differences to actual ECMWF wind larger than −3 m/s, in January and February at 200 hPa. At 100 hPa and 300 hPa, this bias is distinctly smaller.

In the lower stratosphere at high latitudes, the bias of RO-derived wind exhibits an annual cycle with opposite sign for geostrophic and gradient wind. Due to the lack of centrifugal terms in the geostrophic approximation, larger differences to actual winds occur in regions of strong local curvature. Geostrophic

Table 1. Seasonal Mean RO Geostrophic Wind Speed V_{geo} and RO Gradient Wind Speed V_{grad} (Both in m/s) and Their Differences to ECMWF (ΔV_{geo} and ΔV_{grad}; After the Slash, in m/s) for December, January, February (DJF, NH Winter) and June, July, August (JJA, SH Winter) at Pressure Levels 200 hPa and 20 hPa, for 10° Latitude Bands Within 85°N/S and 15°N/S

	DJF, 200 hPa		JJA, 200 hPa		DJF, 20 hPa		JJA, 20 hPa	
	$V_{geo}/\Delta V_{geo}$	$V_{grad}/\Delta V_{grad}$	$V_{geo}/\Delta V_{geo}$	$V_{grad}/\Delta V_{grad}$	$V_{geo}/\Delta V_{geo}$	$V_{grad}/\Delta V_{grad}$	$V_{geo}/\Delta V_{geo}$	$V_{grad}/\Delta V_{grad}$
75°N–85°N	4.4/−0.5	4.2/−0.7	2.7/−0.2	2.6/−0.3	16.5/+0.3	14.1/−2.1	2.6/−0.1	2.7/−0.1
65°N–75°N	7.3/−0.4	7.1/−0.7	5.2/−0.4	5.1/−0.5	26.3/+1.5	24.1/−0.7	4.9/−0.3	5.0/−0.2
55°N–65°N	11.2/−0.2	10.9/−0.5	8.5/−0.3	8.4/−0.5	26.7/+2.5	24.9/+0.8	6.1/−0.2	6.2/−0.1
45°N–55°N	18.6/−0.0	18.0/−0.6	16.9/−0.6	16.4/−1.1	18.7/+2.7	17.8/+1.8	7.4/−0.1	7.5/+0.0
35°N–45°N	31.8/+0.0	30.3/−1.5	20.0/+0.2	19.4/−0.4	9.0/+1.9	8.6/+1.5	10.8/−0.0	11.0/+0.2
25°N–35°N	41.4/−0.2	39.3/−2.4	8.7/+1.5	8.5/+1.3	4.1/+0.2	4.0/+0.1	17.2/−0.6	17.6/−0.2
15°N–25°N	28.4/+2.9	27.5/+2.0	3.0/−0.2	3.1/−0.1	3.3/−0.1	3.3/−0.1	22.6/−1.4	23.2/−0.8
15°S–25°S	9.3/+2.0	9.1/+1.9	29.0/+3.2	28.0/+2.2	18.9/−1.1	19.4/−0.6	4.7/−0.2	4.7/−0.2
25°S–35°S	20.5/+0.4	19.9/−0.2	40.2/−0.8	38.4/−2.7	13.4/−0.1	13.7/+0.2	9.2/+1.3	9.0/+1.1
35°S–45°S	27.8/+1.0	26.8/−0.1	31.3/+0.3	30.0/−1.1	8.8/−0.1	9.0/+0.1	30.6/+3.3	29.2/+1.9
45°S–55°S	29.3/−0.5	27.9/−1.9	27.6/+0.3	26.3/−0.9	5.5/−0.3	5.5/−0.2	58.1/+5.7	53.1/+0.7
55°S–65°S	18.2/−0.7	17.4/−1.4	22.9/−0.5	21.8/−1.6	3.9/−0.0	4.0/+0.0	67.1/+5.8	59.4/−2.0
65°S–75°S	7.3/−0.0	7.1/−0.3	13.0/−0.4	12.4/−1.0	3.7/−0.0	3.7/−0.0	46.6/+4.0	41.1/−1.5
75°S–85°S	2.9/−0.3	2.8/−0.4	5.1/−0.7	4.9/−0.9	2.1/−0.0	2.1/−0.0	20.0/+1.4	17.9/−0.8

wind speed thus clearly overestimates actual wind in the winter lower stratosphere. This bias peaks in August, when it can be up to about 10 m/s at 10 hPa, where wind speeds reach 80 m/s. Gradient winds are significantly less biased, but they underestimate actual wind speed by up to 4 m/s. This bias is largest in August and September.

In order to quantify the accuracy and remaining biases of RO-derived winds in an overall way, Table 1 summarizes results for December, January, February (DJF, NH winter) and June, July, August (JJA, SH winter). Table 1 clearly reveals that seasonal biases rarely exceed 2 m/s in absolute terms and, for larger biases, they rarely exceed 10% in relative terms.

4. Summary and Conclusions

We have used monthly mean sampling error-corrected geopotential height fields on isobaric surfaces (about 190 levels covering 800 hPa to 3 hPa) from radio occultation (RO) measurements and computed geostrophic and gradient wind fields at ~500 km horizontal resolution outside the tropics over 2007 to 2012. RO data feature a unique combination of advantages for this purpose including (i) geopotential height being accurately obtained as vertical coordinate jointly with an accurate retrieval of pressure, (ii) very high vertical resolution, and (iii) global coverage. Best quality of RO geopotential height on isobaric surfaces is obtained in the upper troposphere and lower stratosphere (UTLS) region.

We showed that RO-derived geostrophic and gradient wind fields clearly capture key wind features in the troposphere and lower stratosphere, with differences to actual wind from European Centre for Medium-Range Weather Forecasts (ECMWF) analysis fields being, in general, smaller than 2 m/s. In regions with very high wind speeds such as the upper tropospheric subtropical jet and the stratospheric polar night jet, RO winds exhibit some biases.

Negative biases up to 10 m/s (RO underestimating actual wind speeds) close to the subtropical jet are associated with the geostrophic and gradient wind assumptions. In the subtropical troposphere this bias tends to be smaller for geostrophic wind than for gradient wind, i.e., geostrophic wind better approximates true wind close to the subtropical jet. RO geostrophic winds close to the stratospheric polar night jet, however, feature a positive bias up to 10 m/s (RO overestimating the strength of the jet when it is strongest in August), which is due to the lack of centrifugal terms in the geostrophic approximation. The RO gradient wind is much less biased in this region (negative biases up to 4 m/s in August and September). Even though these biases are larger than 2 m/s in absolute terms, they rarely exceed 10% in relative terms.

Further improvement might be obtained from iteratively generated balanced winds [*Randel*, 1987], but the nonlinear balance approximation was often found not to converge [*Boville*, 1987; *Verkhoglyadova et al.*, 2014]. Furthermore, in their simulation study *Verkhoglyadova et al.* [2014] found no improved wind estimates after first iteration. Thus, more refined effort is needed to further improve the accuracy of winds from RO geopotential height fields. This would be valuable since effects from RO retrieval errors only were found to be smaller than 2 m/s in the entire troposphere and lower stratosphere.

Notwithstanding these further advances, the RO geostrophic and gradient winds already well capture all general wind field patterns, which enables to use the data, for example, to study the dynamics of jet streams under climate variability and change. Overall, the RO wind fields provide new three-dimensional information of high quality on troposphere and stratosphere dynamics, for the benefit of monitoring the climate from weekly to decadal scales.

Acknowledgments

We are grateful to the UCAR/CDAAC and WEGC RO processing team members at WEGC, especially to M. Schwärz and J. Fritzer for their contributions to OPS system development and operations. Furthermore, we thank ECMWF (Reading, UK) for providing access to analysis data. This work was funded by the Austrian Science Fund (FWF) under grant T620-N29 (DYNOCC).

Paul Williams thanks Olga Verkhoglyadova and one anonymous reviewer for their assistance in evaluating this paper.

References

Anthes, R. A. (2011), Exploring Earth's atmosphere with radio occultation: Contributions to weather, climate, and space weather, *Atmos. Meas. Tech.*, *4*, 1077–1103, doi:10.5194/amt-4-1077-2011.

Anthes, R. A., et al. (2008), The COSMIC/FORMOSAT-3 mission: Early results, *Bull. Am. Meteorol. Soc.*, *89*(3), 313–333, doi:10.1175/BAMS-89-3-313.

Boville, B. A. (1987), The validity of the geostrophic approximation in the winter stratosphere and troposphere, *J. Atmos. Sci.*, *44*, 443–457, doi:10.1175/1520-0469(1987)044<0443:TVOTGA>2.0.CO;2.

Foelsche, U., B. Scherllin-Pirscher, F. Ladstädter, A. K. Steiner, and G. Kirchengast (2011), Refractivity and temperature climate records from multiple radio occultation satellites consistent within 0.05%, *Atmos. Meas. Tech.*, *4*, 2007–2018, doi:10.5194/amt-4-2007-2011.

Hajj, G. A., C. O. Ao, B. A. Iijima, D. Kuang, E. R. Kursinski, A. J. Mannucci, T. K. Meehan, L. J. Romans, M. de la Torre Juarez, and T. P. Yunck (2004), CHAMP and SAC-C atmospheric occultation results and intercomparisons, *J. Geophys. Res.*, *109*, D06109, doi:10.1029/2003JD003909.

Harada, Y., A. Goto, H. Hasegawa, N. Fujikawa, H. Naoe, and T. Hirooka (2010), A major stratospheric sudden warming event in January 2009, *J. Atmos. Sci.*, *67*, 2052–2069, doi:10.1175/2009JAS3320.1.

Ho, S.-P., et al. (2012), Reproducibility of GPS radio occultation data for climate monitoring: Profile-to-profile inter-comparison of CHAMP climate records 2002 to 2008 from six data centers, *J. Geophys. Res.*, *117*, D18111, doi:10.1029/2012JD017665.

Holton, J., and G. J. Hakim (2012), *An Introduction to Dynamic Meteorology*, vol. 5, Acad. Press, New York.

Kursinski, E. R., G. A. Hajj, J. T. Schofield, R. P. Linfield, and K. R. Hardy (1997), Observing Earth's atmosphere with radio occultation measurements using the Global Positioning System, *J. Geophys. Res.*, *102*(D19), 23,429–23,465, doi:10.1029/97JD01569.

Leroy, S. S. (1997), Measurements of geopotential heights by GPS radio occultation, *J. Geophys. Res.*, *102*(D6), 6971–6986.

Lieberman, R. S. (1999), The gradient wind in the mesosphere and lower thermosphere, *Earth Planets Space*, *51*, 751–761.

Oberheide, J., G. A. Lehmacher, D. Offermann, K. U. Grossmann, A. H. Manson, C. E. Meek, F. J. Schmidlin, W. Singer, P. Hoffmann, and R. A. Vincent (2002), Geostrophic wind fields in the stratosphere and mesosphere from satellite data, *J. Geophys. Res.*, *107*(D23), 8175, doi:10.1029/2001JD000655.

Pirscher, B., U. Foelsche, B. C. Lackner, and G. Kirchengast (2007), Local time influence in single-satellite radio occultation climatologies from Sun-synchronous and non-Sun-synchronous satellites, *J. Geophys. Res.*, *112*, D11119, doi:10.1029/2006JD007934.

Randel, W. J. (1987), The evaluation of winds from geopotential height data in the stratosphere, *J. Atmos. Sci.*, *44*(20), 3097–3120.

Scherllin-Pirscher, B., G. Kirchengast, A. K. Steiner, Y.-H. Kuo, and U. Foelsche (2011), Quantifying uncertainty in climatological fields from GPS radio occultation: An empirical-analytical error model, *Atmos. Meas. Tech.*, *4*, 2019–2034, doi:10.5194/amt-4-2019-2011.

Schmetz, J., K. Holmlund, J. Hoffman, B. Strauss, B. Mason, V. Gaertner, A. Koch, and L. van de Berg (1993), Operational cloud-motion winds from Meteosat infrared images, *J. Appl. Meteorol.*, *32*, 1206–1225, doi:10.1175/1520-0450(1993)032<1206:OCMWFM>2.0.CO;2.

Schwärz, M., B. Scherllin-Pirscher, G. Kirchengast, J. Schwarz, F. Ladstädter, J. Fritzer, and J. Ramsauer (2013), Multi-mission validation by satellite radio occultation, *Final report for ESA/ESRIN No. 01/2013*, Wegener Center, Univ. of Graz, Graz, Austria.

Smith, L., and J. C. Gille (2014), Validation of the Aura High Resolution Dynamics Limb Sounder geopotential heights, *Atmos. Meas. Tech.*, *7*, 2775-2785, doi:10.5194/amt-7-2775-2014.

Steiner, A. K., B. C. Lackner, F. Ladstädter, B. Scherllin-Pirscher, U. Foelsche, and G. Kirchengast (2011), GPS radio occultation for climate monitoring and change detection, *Radio Sci.*, *46*, RS0D24, doi:10.1029/2010RS004614.

Steiner, A. K., et al. (2013), Quantification of structural uncertainty in climate data records from GPS radio occultation, *Atmos. Chem. Phys.*, *13*, 1469–1484, doi:10.5194/acp-13-1469-2013.

Verkhoglyadova, O., S. Leroy, and C. Ao (2014), Estimation of winds from GPS radio occultations, *J. Atmos. Oceanic Technol.*, doi:10.1175/JTECH-D-14-00061.1.

Wickert, J., et al. (2001), Atmosphere sounding by GPS radio occultation: First results from CHAMP, *Geophys. Res. Lett.*, *28*(17), 3263–3266.

Wickert, J., G. Beyerle, R. König, S. Heise, L. Grunwaldt, G. Michalak, C. Reigber, and T. Schmidt (2005), GPS radio occultation with CHAMP and GRACE: A first look at a new and promising satellite configuration for global atmospheric sounding, *Ann. Geophys.*, *23*, 653–658.